Cloud Droplet Growth by Condensation in Homogeneous Isotropic Turbulence

ALESSANDRA S. LANOTTE

CNR, Istituto di Scienze dell'Atmosfera e del Clima, Rome, and Istituto Nazionale di Fisica Nucleare, Lecce, Italy

AGNESE SEMINARA

School of Engineering and Applied Sciences, Harvard University, Cambridge, Massachusetts

FEDERICO TOSCHI

Department of Physics, and Department of Mathematics and Computer Science, Eindhoven University of Technology, Eindhoven, Netherlands, and Istituto per le Applicazioni del Calcolo, Rome, and Istituto Nazionale di Fisica Nucleare, Ferrara, Italy

(Manuscript received 23 June 2008, in final form 2 November 2008)

ABSTRACT

The growth of cloud droplets by diffusion of water vapor in a three-dimensional homogeneous isotropic turbulent flow is considered. Within a simple model of advection and condensation, the dynamics and growth of millions of droplets are integrated. A droplet-size spectra broadening is obtained and it is shown to increase with the Reynolds number of turbulence by means of two series of direct numerical simulations at increasing resolution. This is a key point toward a proper evaluation of the effects of turbulence for condensation in warm clouds, where the Reynolds numbers typically achieve extreme values. The obtained droplet spectral broadening as a function of the Reynolds number is shown to be consistent with dimensional arguments. A generalization of this expectation to Reynolds numbers not accessible by direct numerical simulation (DNS) is proposed, yielding upper and lower bounds to the actual size spectra broadening. It is argued that the lower bound is the relevant limit at high Reynolds numbers. A further DNS matching the large scales of the system suggests consistency of the picture drawn. The assumptions underlying the model are expected to hold up to spatial scales on the order of 100 m; no direct comparison with in situ measures is possible. Additional effort is needed to evaluate the impact of this effect for condensation in more realistic cloud conditions.

1. Introduction

The growth of droplets by condensation is a long-standing problem of cloud physics (Pruppacher and Klett 1997), meteorology (see, e.g., Houghton et al. 2001), medicine (Martonen 2000), and engineering (Zhao et al. 1999). A fundamental understanding of key issues, such as the turbulent mixing inside clouds or the interaction of turbulence with microphysics, is important for a variety of applications (e.g., the parameterization of small scales in large-scale models, the analysis of radiative transfer through clouds, the accurate prediction of the initiation of precipitation). At a Reynolds number approaching $\mathrm{Re} \sim 10^8$, turbulence is known to be highly fluctuating, with a substantial probability of velocity differences far exceeding the standard deviation (see, e.g., Frisch 1995). Such behavior, with large variations at progressively smaller scales, is even stronger for scalars advected by turbulent flows, with the formation of clifflike structures in the field (see, e.g., Shraiman and Siggia 2000). This means that droplets coming close to one another might have previously experienced disparate conditions, and mean field–type expectations become questionable. These concepts have a long history in cloud physics: turbulence is believed to play a role both in collision processes and in condensation [see Shaw (2003) for a review]. In this work we will focus particularly on the latter process.

Condensation is a fundamental process for the early stages of cloud evolution when droplets are few microns in size and collisions are not yet effective. In

Corresponding author address: Agnese Seminara, Harvard University, School of Engineering and Applied Sciences, 29 Oxford Street, Cambridge, MA 02138.
E-mail: seminara@seas.harvard.edu

DOI: 10.1175/2008JAS2864.1

situ measurements of droplet-size spectra in warm clouds at this early stage revealed the presence of a wide variety of sizes (Warner 1969). This feature of the condensational growth still eludes full theoretical understanding despite the number of different mechanisms proposed. In fact, provided that all droplets grow in similar ambient conditions, small droplets are expected to grow faster than large ones, thus narrowing the size distribution. This yields the still unsolved problem of the bottleneck between condensation and collision–coalescence. Indeed, collision rates can be strongly reduced in the presence of narrow droplet-size spectra. Many efforts have been deployed to explain the observed widths of droplet spectra, pointing to the role of entrainment and mixing with noncloudy air occurring in the regions of the cloud near the boundaries (see, e.g., Blyth 1993) or the local variability of environmental conditions due to droplet evaporation (Andrejczuk et al. 2004; Malinowski et al. 1998; Korczyk et al. 2006). The general conclusion is that these microscopic fluctuations influence the process of mixing occurring at the interface between cloud and clear air, which is not the object of the present work.

On the other hand, criticism of the underlying assumption of uniformity in the environmental conditions has been raised since the 1960s, when the theory of stochastic condensation was first proposed (see, e.g., Mazin 1968; Levin and Sedunov 1966; Bartlett and Jonas 1972). The spectral broadening arising as a consequence of turbulent fluctuations in the environment has been analyzed several times in the literature by means of idealized analytic models (see, e.g., Srivastava 1989; Cooper 1989). More recently, numerical approaches have been used to test some of these ideas (Vaillancourt et al. 2002; Celani et al. 2005; Lasher-Trapp et al. 2005). However, results are not conclusive, particularly because direct numerical simulation (DNS) of cloud turbulence cannot resolve the entire range of active degrees of freedom. As a consequence of the spatial structure of the turbulent fields, DNS can either focus on large-scale fluctuations, as done by Celani et al. (2005, 2007), or resolve the small-scale features as in Vaillancourt et al. (2001, 2002). The two choices are mutually exclusive because of finite computing resources and both have strong and weak points, as discussed in section 2. Here we will try to take advantage of both these approaches to achieve a deeper understanding of the role of turbulence as a broadening mechanism in adiabatic cloud cores. Notice that size distributions broader than the adiabatic reference from the uniform parcel model have been measured in adiabatic cloud cores as well (Brenguier and Chaumat 2001).

In a nutshell, in this paper we focus on the growth of cloud droplets by diffusion of water vapor in a turbulent environment, neglecting possible effects due to entrainment, mixing, or droplet properties such as salinity or curvature [on this point see, e.g., Korolev and Mazin (2003)]. We first evaluate the spreading of the droplet-size distribution through two series of direct numerical simulations at increasing resolution, matching the small-scale features. Not surprisingly, each single DNS gives a small degree of spreading, as already pointed out in previous DNS focusing on small rising fluid parcels (Vaillancourt et al. 2002). This is consistent with the fact that in a small cloud with limited vertical updraft, the fluctuations in the supersaturation are small as well. However, this only tells us that turbulence at the smallest scales alone fails to reproduce the observed broadening of the droplet-size distributions.

Then we evaluate the dependence of the size spectra broadening on the turbulent Reynolds number (i.e., on the range of spatial scales resolved). The broadening is found to increase with the Reynolds number of turbulence. Because the Reynolds numbers of real cloud turbulence are several orders of magnitude larger than those described by DNS, this increase must be accounted for when assessing the role of turbulence for condensation in clouds. On the basis of a dimensional analysis, we derive upper and lower bounds on the trend of the spectral broadening as a function of the Reynolds number. The upper bound is obtained by neglecting the vapor depletion due to condensation onto cloud droplets. We argue that this should be significant at small Reynolds numbers, and we show that it is consistent with the two series of DNS performed. We then reason that the lower bound, where the vapor fluctuations are considered immediately depleted for condensation/evaporation, should be more significant at high Reynolds numbers. A further DNS matching the large scales of the problem suggests consistency with the argument.

The paper is organized as follows: In section 2 we introduce the model for the time evolution of the vapor field and the droplets advected by the turbulent airflow. Section 2a is devoted to the numerical approach, whereas section 3 describes DNS details and the range of parameters explored. Results concerning the spreading of the droplet-size spectrum are presented in section 4, and their implications for large Reynolds numbers are discussed in section 5. Conclusions and perspectives follow in section 6.

2. Model equations

We focus on a turbulent velocity field advecting water vapor and droplets. The latter undergo size changes for

evaporation or condensation of the surrounding vapor. The three-dimensional velocity field of in-cloud air ($\mathbf{v}$) evolves according to the Navier–Stokes equations for an incompressible flow

$$\partial_t \mathbf{v} + \mathbf{v}\cdot\nabla\mathbf{v} = -\frac{\nabla p}{\rho_a} + \nu\Delta\mathbf{v} + \mathbf{f}, \quad \text{where } \nabla\cdot\mathbf{v} = 0, \quad (1)$$

where p is the pressure, ρ_a is the air density, and ν is the air kinematic viscosity. The vector $\mathbf{f}$ represents an external statistically homogeneous and isotropic forcing, providing a turbulent stationary flow. Because we neglect thermal convection (i.e., temperature is not explicitly considered), the energy balance only includes kinetic energy and viscous dissipation. However, latent heat effects on the vapor field are taken into account in the equation for the supersaturation field, as clarified below.

In the spirit of classical Kolmogorov theory, turbulence can be considered statistically homogeneous and isotropic only in the limit of very large Reynolds number and at the smallest scales of motion (Frisch 1995). As for cloud physics, in Vaillancourt and Yau (2000) the authors argue that large-scale thermal gradients can be neglected in warm-cloud cores for spatial scales up to $L \sim 100$ m. Additionally, anisotropy is produced through buoyancy by microscopic temperature fluctuations coupled with droplet evaporation. This effect can be important for cloud–clear air mixing (see Korczyk et al. 2006; Malinowski et al. 1998; Andrejczuk et al. 2004), which we are here ignoring. We remark that previous numerical studies in two dimensions (Celani et al. 2005, 2007) suggest that the qualitative effects of turbulence on droplet size spectra do not rely specifically on the statistical details of the flow regime analyzed.

Water vapor molecules carried by the turbulent velocity field are the source for droplet growth by condensation. The relevant quantity for condensation/evaporation is the supersaturation, defined as $s = e/e_s - 1$, where e and e_s are the vapor pressure and the saturation vapor pressure respectively; droplets grow in regions with higher supersaturation and evaporate in regions with lower supersaturation values, as described by Eq. (4).

For the sake of generality, we adopt here a simple generalization of the well-known model for the supersaturation time evolution proposed in Twomey (1959). Whereas Twomey considered a one-dimensional equation for the time-dependent supersaturation function, here we consider s as a field $s(\mathbf{x}, t) = e/e_s\ (\mathbf{x}, t) - 1$, fluctuating both in space and time. Note that because there is no mean vertical velocity in our model, supersaturation $s(\mathbf{x}, t)$ has a zero mean value and is allowed to fluctuate from positive to negative values. Supersaturated and undersaturated regions can coexist at the same time in the considered volume. The generalization of Twomey's equation for the supersaturation field is an advection–diffusion equation:

$$\partial_t s + \mathbf{v}\cdot\nabla s = \kappa\Delta s + A_1 w - \frac{s}{\tau_s}, \quad (2)$$

where κ is the molecular diffusivity of water vapor in air and $w(\mathbf{x}, t)$ is the vertical component of the turbulent velocity field $\mathbf{v}$. Note that this equation is only approximately true because temperature and moisture have slightly different diffusion constants. In Vaillancourt et al. (2001) the authors separately integrate the equations for temperature and moisture to obtain the supersaturation. Another difference with respect to the cited work is that here the average supersaturation vanishes, so that mean growth of the droplets population is not considered.

The scalar field s is considered to be passive; that is, we are neglecting the compositional effects of vapor on the buoyancy forces acting on the flow, which are generally thought to be small (see Stevens 2005). The term $A_1 w$ acts as a source/sink term of supersaturation resulting from the variation in temperature and pressure with height. By standard assumptions (see, e.g., Politovich and Cooper 1988; Pruppacher and Klett 1997) it turns out that $A_1 = Lg/(R_v c_p T^2) - g/(R_a T)$, where L is the latent heat of evaporation, R_v and R_a are the gas constants for vapor and dry air, c_p is the specific heat at constant pressure, and g is the gravitational acceleration.

The term $-s/\tau_s$ accounts for the double effect of condensation/evaporation on supersaturation: on one hand, the phase change directly modifies the water vapor content; on the other, it locally modifies temperature—and therefore supersaturation—because of absorption or release of latent heat. The parameter τ_s is the phase relaxation time scale of the supersaturation and depends locally on the concentration and size of droplets:

$$\tau_s^{-1} = \frac{4\pi\rho_w A_2 A_3}{V}\sum_{i=1}^{n} R_i, \quad (3)$$

where R_i are the radii of the n droplets inside the considered volume V; A_2 is a function of thermodynamic parameters, and we consider it constant as shown in Table 1 (see, e.g., Pruppacher and Klett 1997); ρ_w is the water density; and A_3 is the rate of droplet radius growth by condensation [see Eq. (4)]. The role of τ_s is of crucial importance as already pointed out in several previous works (see, e.g., Clark and Hall 1979).

TABLE 1. Reference values for the physical parameters used in the numerical experiments. The air kinematic viscosity is $\nu \approx 0.15\ \mathrm{cm^2\ s^{-1}}$, and the molecular diffusivity of water vapor in air is $\kappa \approx 10^{-5}\ \mathrm{m^2\ s^{-1}}$; A_1 is the global supersaturation gradient and A_2 and A_3 are functions of the ambient thermodynamic parameters. As reference values for the temperature and pressure, we used $T = 283$ K and $p = 1000$ hPa. The values of the vapor phase relaxation time τ_s, droplet radius R, and Stokes number St correspond to averages on the initial condition of droplet population.

Label	A_1 ($\mathrm{m^{-1}}$)	A_2 ($\mathrm{kg^{-1}\ m^3}$)	$A3$ ($\mu\mathrm{m^2\ s^{-1}}$)	N_{drops}/V ($\mathrm{cm^{-3}}$)	LWC ($\mathrm{g\ m^{-3}}$)	τ_s (s)	R (μm)	St
Series 1	5×10^{-4}	350	50	130	1.2	2.5	13	3.5×10^{-2}
Series 2	5×10^{-4}	350	50	130	0.07	7	5	5×10^{-3}

In the presence of a mean updraft velocity $\overline{W}$ and if variations of τ_s with the mean radius are negligible, the mean supersaturation approaches its quasi-steady value $S_{\mathrm{qs}} \approx A_1 \overline{W} \tau_s$ at times longer than τ_s. Because here we consider vanishing mean updrafts, we will apply the concept of quasi-steady state to the fluctuations of s rather than to its mean value.

The remarkable feature of the simple model represented by Eqs. (1) and (2) is that despite its simplicity, it allows us to identify nontrivial mechanisms leading to the spreading of the size spectra.

Given the evolution equation for the Eulerian turbulent fields, we can now introduce the Lagrangian dynamics of cloud droplets and the time evolution of their radii. A complete description of the relation between the water vapor and the size of a spherical droplet would imply an integral equation for the local dynamics occurring at the droplet surface. Note, however, that the typical time scales associated with the diffusional growth of an isolated droplet are much smaller than the fastest time scale associated with turbulent changes in the ambient conditions (see Vaillancourt et al. 2001). By assuming instantaneous water vapor equilibrium, we end up with the standard equation for the diffusional growth of the ith droplet (see, e.g., Pruppacher and Klett 1997):

$$\frac{dR_i(t)}{dt} = A_3 \frac{s[\mathbf{X}_i(t), t]}{R_i(t)}. \tag{4}$$

Here A_3 is a function of the local conditions, air temperature, and pressure and is assumed to be constant throughout the entire volume (variations of this parameter with temperature in typical warm cloud conditions are smaller than 3%). Its detailed expression can be found in Pruppacher and Klett (1997); here we just mention that its value is derived neglecting curvature and salinity effects, as is appropriate for the droplet sizes considered in this study (>5 μm).

According to Eq. (4), the growth rate varies from a droplet to another because it depends on the supersaturation fluctuation $s[\mathbf{X}_i(t), t]$ measured along the trajectory $\mathbf{X}_i(t)$ of the single droplet. Because of turbulent transport, initially close droplets separate very rapidly and eventually experience disparate values of supersaturation throughout the entire cloud volume. This is the most important difference with respect to Twomey's model where all the droplets are exposed to the same supersaturation value.

Cloud droplets can be described as independent Stokes particles, whose trajectories $\mathbf{X}_i(t)$ and velocities $\mathbf{V}_i(t)$ evolve according to

$$\frac{d\mathbf{X}_i(t)}{dt} = \mathbf{V}_i(t) \quad \text{and} \tag{5}$$

$$\frac{d\mathbf{V}_i(t)}{dt} = -\frac{\mathbf{V}_i(t) - \mathbf{v}[\mathbf{X}_i(t), t]}{\tau_d^i} + g\hat{\mathbf{z}}. \tag{6}$$

Here $\mathbf{v}[\mathbf{X}_i(t), t]$ is the fluid velocity at the particle position; $\tau_d^i(t) = R_i^2(t)/(3\nu\beta)$ is the particle response time (or Stokes time); $\beta = 3\rho_a/(\rho_a + 2\rho_w) \approx 3\rho_a/(2\rho_w)$ is proportional to the air/water density ratio; and g is the gravitational acceleration. Equations (5) and (6), derived from the more general treatment of Maxey and Riley (1983), are valid for dilute suspensions of small spherical heavy particles. These hypothesis are well verified during the condensation stage [as discussed, e.g., in Vaillancourt and Yau (2000)]. Because collisions are still negligible in the range of parameters considered, droplet–droplet hydrodynamical interactions are ignored. Droplet back reaction onto the airflow is neglected as well because the mass loading and the ratio between droplet size and Kolmogorov scale are much smaller than 1 (one-way coupling model). Notice that gravitational acceleration is included in our model, although we shall not discuss the interplay between sedimentation and turbulence in our simulations (see, e.g., Grabowski and Vaillancourt 1999). This is left for future studies.

Numerical procedures

Equations (1) and (2) are integrated using pseudospectral methods with 2/3-rule dealiasing (Orszag 1971) in a triply periodic box. The fully parallelized code relies on the use of fast Fourier transforms (FFTs) for an

efficient evaluation of the advection terms in Fourier space. We used the open-source Fastest Fourier Transform in the West (FFTW) 2.1.5 libraries.

Unless stated differently, molecular viscosity (and diffusivity) is chosen to match the Kolmogorov length scale η with the grid spacing $\eta \simeq \delta x$: this choice ensures a good resolution of the turbulent fluctuations at any scale and prevents oscillations due to truncation of small-scale motion (see Spyksma et al. 2006). For both equations, time stepping is done using a second-order Adam–Bashforth (AB) scheme, and in particular the time step is chosen to accurately resolve the smallest turbulent fluctuations and the fluid acceleration.

In Eq. (1), kinetic energy is injected at an average rate ε by keeping constant the total energy in each of the first two wavenumber shells (Chen et al. 1993). The scalar field is forced by the assigned gradient A_1; the term $-s/\tau_s$ does not contribute as long as droplets are not injected into the flow. In our DNS, we consider each droplet to affect the value of τ_s in the eight nodes of the grid cell surrounding its position. The weight of the contribution to each node is calculated via a three-linear extrapolation.

Droplet dynamics is also fully parallel. Droplet motion [Eqs. (5) and (6)] and radius evolution are integrated with a second-order AB scheme. To obtain droplet velocity from Eq. (6), the underlying flow velocity at the droplet position has to be computed. This is done via a linear interpolation in the three spatial directions (Yeung and Pope 1988), which was demonstrated to be adequate to obtain well-resolved particle acceleration. Similarly, we compute the vapor field $s[\mathbf{X}(t)]$ at the droplet position to evolve the radius.

3. Numerical simulations and range of parameters

As mentioned earlier, DNS of cloud physics present a major problem: there are a vast number of degrees of freedom that cannot be described simultaneously. Turbulence is organized in spatial structures of typical sizes ranging from the large-scale L of thousands of meters down to the Kolmogorov scale η (typically $\sim$1 mm). Similarly, the time scales range from thousands down to fractions of a second. Within this highly turbulent medium, a population of 10^{14}–10^{18} droplets evolves. Moreover, even if droplets are much smaller than any turbulent eddy, their trajectory spans the whole range of turbulent scales. This yields correlations with the fluctuations of the vapor field [see Celani et al. (2005, 2007)] and with the structures of the velocity field as shown, for example, in Eaton and Fessler (1994). Therefore, turbulent motion at any scale plays a significant role in droplet dynamics. However, when dealing with experiments *in silico*, because of computational limitations it is compulsory to choose a setting that describes only a limited range of spatial structures in the system.

Recent results, reported in Celani et al. (2005, 2007), of direct numerical simulations in two dimensions pointed out the importance of the large-scale fluctuations of the vapor field. These provide a strongly variable environment for droplet evolution, resulting in a spreading of the droplet-size spectrum. In such context, the small scales of turbulence cannot be resolved and the analysis is limited to a statistically representative subset of the whole population of droplets. In Vaillancourt et al. (2002), the complementary setting is adopted: by concentrating on a small rising parcel, the authors can consistently describe the droplet evolution in full detail. This approach provides small fluctuations that eventually produce a limited degree of spreading. Note that the small scales inside a cloud are the end point of a turbulent cascade involving a wide range of interacting spatial and temporal scales. Consequently, they are not independent from the large scales, suggesting that approaches that separate small from large scales might fail in reproducing turbulent effects. In this respect, because DNSs do not describe the whole inertial range of cloud turbulence, the fluid-parcel approach does not represent a small portion of a big cloud, but rather a very small cloud.

Here we wish to investigate how turbulence effects change with the Reynolds number by merging the two complementary approaches above mentioned. This is a crucial step in assessing the role of turbulence for cloud-droplet condensation, since real cloud turbulence has Reynolds numbers dramatically higher than the simulated flows. To this purpose, we start by performing two series of direct numerical simulations at increasing resolution. The grid spacing Δx of each simulation corresponds to about 1 mm. By progressively increasing the number of grid points for each spatial direction, we can resolve larger integral scales L, defining the size of the cloud. More precisely, we consider two series of four numerical experiments, labeled runs A, B, C, and D, with 64^3, 128^3, 256^3, and 512^3 grid points respectively. The two series of simulations have different initial liquid water content (LWC): $\sim$1.2 g cm^{-3} for series 1 and $\sim$0.07 g cm^{-3} for series 2. The integral scale of the system varies from $L \sim 9$ cm up to $L \sim 70$ cm. The microscale Reynolds numbers $\mathrm{Re}_\lambda \approx \sqrt{15\,\mathrm{Re}}$ (see Frisch 1995) range from $\mathrm{Re}_\lambda \sim 40$ to $\mathrm{Re}_\lambda \sim 185$, which represents the state of the art for DNS in cloud physics. The ratio between the air kinematic viscosity and the vapor molecular diffusivity, also called the Schmidt number, is $\mathrm{Sc} = \nu/\kappa = 1$, so that the flow and the scalar dissipative scales are of the same order. Kinetic energy dissipation

TABLE 2. Parameters of the DNS, series 1 and 2. From left to right: number of grid points N^3, integral scale L, large-scale eddy turnover time T_L, microscale Reynolds number Re_λ, average kinetic energy dissipation rate ϵ, Kolmogorov spatial scale η, Kolmogorov time scale τ_η, initial supersaturation standard deviation σ_s^0, velocity standard deviation v_{rms}, and number of droplets N_{drops}.

Label	N^3	L (cm)	T_L (s)	Re_λ	ε (m^2 s^{-3})	η (cm)	τ_η (s)	σ_s^0 (%)	v_{rms} (m s^{-1})	N_{drops} ($\times 10^5$)
A	64^3	9	2.0	40	10^{-3}	0.1	0.1	1.5×10^{-3}	4×10^{-2}	0.93
B	128^3	18	3.5	65	9.0×10^{-4}	0.1	0.1	3.4×10^{-3}	5.0×10^{-2}	8.2
C	256^3	38	5.5	105	10^{-3}	0.1	0.1	6.1×10^{-3}	7.0×10^{-2}	71.2
D	512^3	70	7.6	185	1.1×10^{-3}	0.1	0.1	1.2×10^{-2}	1.0×10^{-1}	320

is chosen to be $\varepsilon \simeq 10^{-3}$ m^2 s^{-3}, which is consistent for clouds with moderate turbulence levels (see Chaumat and Brenguier 2001).

Table 1 shows the reference values of physical parameters such as A_1, A_2, and τ_s used in the numerical experiments; Table 2 lists DNS details for the two series of simulations.

Clearly the process of doubling the resolution, if iterated, would ideally lead to the description of the whole range of scales from η to L appropriate for cloud conditions. Because we can only perform the first few iterations of this process, the next step will be to discuss if this can be extrapolated to give information on Reynolds numbers that are not accessible by DNS. An attempt in this direction will be discussed in detail in section 5.

We obtain a statistically stationary state for the velocity and supersaturation fields with no droplets by integrating Eqs. (1) and (2) for few large-scale eddy turnover times $T_L = L/v_{\mathrm{rms}}$. Figure 1 shows the supersaturation spectrum at the stationary state for run D, where $\mathrm{Re}_\lambda \sim 185$, before particle injection. In agreement with classical Kolmogorov–Obukhov–Corrsin theory (see, e.g., Tennekes and Lumley 1972), this exhibits a $k^{-5/3}$ power law behavior in the Fourier space. Because the scalar spectrum is peaked on the large scales, as the integral scale increases we approach larger and larger fluctuations. We indicate with σ_s^0 the supersaturation standard deviation in the stationary state before droplet injection. In the inset of Fig. 1, we show that σ_s^0 increases linearly with the size of the system as expected from a dimensional balance of terms in Eq. (2) disregarding the term $-s/\tau_s$, yielding $\sigma_s^0 \sim A_1 L$. The above fit also provides the proportionality constant that turns the dimensional relation in a prediction. Such increase can be understood from the physical viewpoint: larger cloud sizes correspond to larger displacements and stronger adiabatic cooling. This directly provides larger fluctuations in the vapor field through the term $A_1 w$ in Eq. (2). When droplets are injected in the flow, this picture changes and the supersaturation fluctuations are modified as described below.

Note that we are not describing droplet nucleation onto cloud condensation nuclei: our simulations start with droplets already activated. Therefore, there is no conservation of the total water content at time zero, when the droplets are injected in the volume. However, because the total water conservation is conserved at any later time, we consider this irrelevant for the results of the simulations performed.

4. Spectral broadening

Once the steady state has been attained, a monodispersed population of droplets with initial radius $R_i = 13$ μm for series 1 and $R_i = 5$ μm for series 2 is injected into the flow. The complete system—flow, scalar, and droplets—has been studied, at the largest resolution, for about two large-scale eddy turnover times. Longer time integrations were performed at lower resolutions. Droplet concentration is for all runs $\approx$130 cm^{-3}, which means

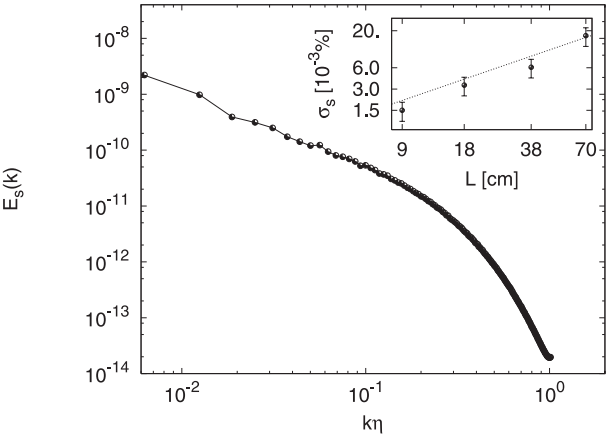

FIG. 1. Log–log plot of the stationary supersaturation spectrum for run D at $\mathrm{Re}_\lambda \sim 200$, before injection of droplets. It shows a $k^{-5/3}$ power law behavior, as expected from Kolmogorov–Obukhov–Corssin theory. The turbulent velocity field also displays a Kolmogorov spectrum (not shown). Inset: log–log plot of the standard deviation of the supersaturation field σ_s^0, measured in the stationary state, vs the size of the system L. The behavior is in agreement with the dimensional prediction $\sigma_s^0 \sim A_1 L$.

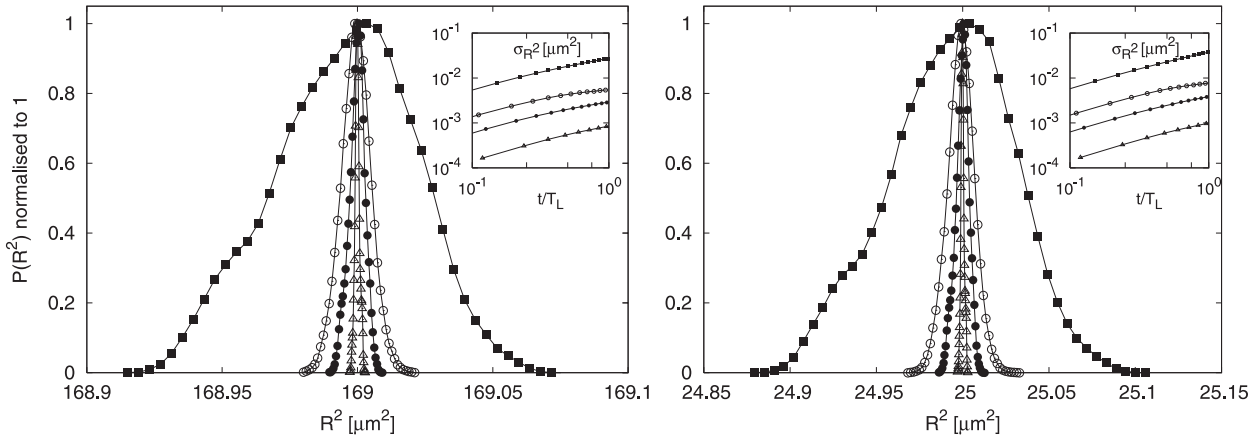

FIG. 2. Droplet square size distribution $P(R^2)$ measured after one large-scale eddy turnover time T_L for the four DNS of series (left) 1 and (right) 2. At increasing the turbulence Reynolds number, we move from inner to outer curves. Symbols are as follows: run A—open triangles, run B—filled dots, run C—open circles, and run D—filled squares. In each run, the droplets' initial size distribution (not shown) is $\delta(R - R_0)$, with $R_0 = 13$ μm for series 1 and $R_0 = 5$ μm for series 2. Each simulation presents a small degree of spreading, which increases with the Reynolds number. Inset: Log–log plot of the time evolution of the standard deviation of the square size distribution σ_{R^2} for runs A–D (from bottom to top). Symbols are as in the main figure.

that, on average, about one out of every two to four cells contains a droplet. In the largest simulation we followed the time evolution of 32 million droplets. Initially, these are distributed randomly in space according to a statistically homogeneous Poisson distribution. The Lagrangian Eqs. (5) and (6) for particle motion are integrated simultaneously with those for the Eulerian fields (1) and (2). Particle initial velocities are set equal to the local fluid velocity.[1]

As the cloud particles are released, they explore the entire volume and experience the range of vapor fluctuations available in the system. In Fig. 2, the droplet square size distributions $P(R^2)$ are shown for runs A–D after one large-scale eddy turnover time for series 1 and series 2. The mean value is constant because $\langle s \rangle = 0$, while a small degree of spreading is present for each simulation, increasing with the size of the cloud. This is due to the fact that when evolving in a larger cloud, droplets are trapped in longer updrafts and downdrafts and therefore experience stronger fluctuations of supersaturation. When dealing with small clouds, the broadening resulting from the different droplet histories is limited, as already pointed out in Vaillancourt et al. (2002), but increases as we consider larger volumes (and larger Re).

A more quantitative measure of the spectral broadening is shown in the inset of Fig. 2. Here we show that for $t \leq T_L$ the standard deviation of the square radii $R^2(t)$ increases linearly in time. Linearity implies that at short time lags droplet surface grows with the vapor fluctuation initially experienced and does not feel the underlying local variations.[2] After few phase relaxation times τ_s have elapsed, the vapor field standard deviation is depleted by droplet absorption, thus slowing down the broadening of droplet size distribution. The mean vapor phase relaxation time—estimated through Eq. (3) with average concentration $\approx$130 drops cm^{-3} and mean radius 13 μm and 5 μm—turns out to be $\approx$2.5 s for series 1 and $\approx$7 s for series 2. Because this time scale is comparable with the eddy turnover time for simulations A–D (see Tables 1 and 2), the supersaturation fluctuations do not change considerably from their initial value during T_L. For this reason, the linear growth of $\sigma_{R^2}(t)$ in time extends to the whole large-scale eddy turnover time T_L and the final spreading, measured at $t = T_L$, is well approximated dimensionally from Eq. (4):

$$\sigma_{R^2}(T_L) \sim A_3 \sigma_s^0 T_L \,. \tag{7}$$

In Fig. 3 the final broadening $\sigma_{R^2}(T_L)$ is shown to increase as a function of the microscale Reynolds number Re_λ characterizing flows A–D. This is another way to show that the increase of updraft/downdraft intensity

[1] Tests have been performed by setting the droplet initial velocity equal to the terminal velocity $v_T = g\tau_d$. We did not observe any significant deviations in the results. Indeed, particles rapidly equilibrate to the flow on a time scale on the order of their response time.

[2] A proportional linear growth is also observed for the standard deviation of droplet radii $R(t)$ (not shown). This is because, given the tiny supersaturation fluctuations, the droplet-size distribution is close to a Gaussian and the mean radius is much larger than the standard deviation. Hence, $\sigma_{R^2}^2 \approx 2\sigma_R^4 + 4\sigma_R^2 \langle R \rangle^2 \approx 4\sigma_R^2 \langle R \rangle^2$.

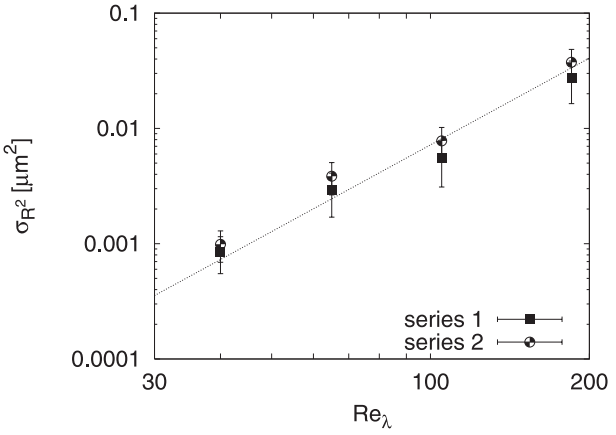

FIG. 3. Log–log plot of the spreading of droplet size distribution $\sigma_{R^2}(T_L)$ for the square radius R^2, measured after one large-scale eddy turnover time T_L as a function of the Reynolds number Re_λ. Data refer to simulations A–D of series 1 (squares) and 2 (circles). For both series, the spreading is larger as the Reynolds number increases because droplets evolve in conditions that are more and more differentiated. The dimensional prediction $\sigma_{R^2} \sim c_1 \mathrm{Re}_\lambda^\xi$ with $\xi = 5/2$ and $c_1 \propto A_1 A_3 \upsilon_\eta \tau_\eta^2$ is shown for comparison (see the text). The extrapolation of this law gives an upper bound to the final spreading for the target cloud of parameters $L = 100$ *m*, $\sigma_s^0 \sim 2\%$, and $\mathrm{Re}_\lambda \sim 4000$–$7000$: $\sigma_{R^2}^{\mathrm{ext}} \sim 200 \pm 100\ \mu\mathrm{m}^2$. A correction of the expectation accounting for vapor depletion caused by droplet feedback gives $\sigma_{R^2}^{\mathrm{ext}} \sim 3.3 \pm 1.6\ \mu\mathrm{m}^2$ for series 1 and $\sigma_{R^2}^{\mathrm{ext}} \sim 9.3 \pm 4.5\ \mu\mathrm{m}^2$ for series 2 (see the text).

enhances the supersaturation fluctuations available and thus droplet differentiation.

The reason why we analyze this dependence is that we would like to generalize it to arbitrary Reynolds numbers, as discussed in section 5. Note that the results of the two series of simulations are remarkably close, pointing once more to a limited role of vapor absorption by condensation at small Reynolds number. The picture will change at larger Reynolds numbers as discussed later.

The relation between final broadening and Reynolds number can be obtained from Eq. (7), which—we emphasize again—is well verified when we consider the spreading at time scales comparable with the phase relaxation time τ_s. To do this, we use the following standard dimensional relations valid for statistically homogeneous and isotropic turbulence (see, e.g., Pope 2000): $T_L \sim \tau_\eta \mathrm{Re}_\lambda$ and $w_{\mathrm{rms}} \sim \upsilon_\eta \mathrm{Re}_\lambda^{1/2}$, where w_{rms} is the root-mean-square value of the vertical component of the velocity field. Remembering from the previous section that the supersaturation fluctuations have initial standard deviation $\sigma_s^0 \sim A_1 L \sim A_1 w_{\mathrm{rms}} T_L$, it is straightforward to show that Eq. (7) yields

$$\sigma_{R^2} \sim A_3 A_1 \upsilon_\eta \tau_\eta^2 \mathrm{Re}_\lambda^{5/2}, \tag{8}$$

based on self-similarity of the growth process during the turbulent regime. In Fig. 3 we show for comparison the dimensional expectation (8).

5. Discussion

It is natural to ask whether this trend can give information on the final broadening achieved at Reynolds numbers higher than $\mathrm{Re}_\lambda = 185$. This point deserves insight because the Reynolds number of real cloud turbulence is several orders of magnitude larger than those described by direct numerical simulations.

At larger Reynolds numbers and large-scale eddy turnover times, droplets significantly absorb the surrounding vapor, so that the initial standard deviation σ_s^0 is no longer a good approximation of $\sigma_s(t)$ at long times. This means that the scaling (8) is an upper bound for the actual spectral broadening at larger Reynolds number. A lower bound can be simply obtained by assuming that droplet feedback on the supersaturation is instantaneous. This is done by estimating the supersaturation fluctuations with their quasi-steady value $\sigma_s^{\mathrm{qs}} \sim A_1 w_{\mathrm{rms}} \tau_s$, coming from the balance of the last two terms on the rhs of Eq. (2). For a discussion of the quasi-steady approximation and its validity see, for example, Politovich and Cooper (1988). Replacing σ_s^0 with the quasi-steady value σ_s^{qs} in the dimensional relation (7), we obtain

$$\sigma_{R^2} \sim A_3 A_1 \upsilon_\eta \tau_\eta \tau_s \mathrm{Re}_\lambda^{3/2}, \tag{9}$$

yielding a correction to the upper bound (8) of a factor τ_s/T_L. As illustrated below, the difference between the two bounds becomes larger and larger as we approach large Reynolds numbers. We will argue that the lower bound is the relevant limit at high Reynolds numbers.

The ratio τ_s/T_L fluctuates both in space and time according to the local properties of both turbulence and droplet population. We can estimate the large-scale eddy turnover time and the Reynolds number through the standard dimensional relations $T_L \sim \tau_\eta \mathrm{Re}_\lambda$ and $\mathrm{Re}_\lambda \sim (L/\eta)^{2/3}$ (see, e.g., Pope 2000). The proportionality constants are estimated by fitting the dimensional relations on the small-scale data, as illustrated in section 3 for σ_s^0. We choose to extrapolate the results to a cloud core of size $L \sim 100$ m, since the homogeneous isotropic scheme is expected to hold at these scales. For this system, the Reynolds number is in the range $\mathrm{Re}_\lambda \approx 4000$–$7000$ and the large-scale eddy turnover time is $T_L \approx 150$ s. In the absence of vapor absorption onto droplets, the upper bound (8) gives $\sigma_{R^2}(T_L) < 200 \pm 100\ \mu\mathrm{m}^2$. The time scale τ_s does not depend on Reynolds but only on the LWC and the droplet density.

If the liquid water content is 1.2 g m^{-3} and there are 130 drops cm^{-3}, then its mean value is $\tau_s \approx 2.5$ s, as in series 1. The extrapolation of the lower bound (9) gives $\sigma_{R^2}(T_L) > 3.3 \pm 1.6\ \mu m^2$. Note that to put error bars on the Reynolds number we consider fluctuations of 25% on its average value. These error bars correspond to the same level of fluctuations for the instantaneous value of the Reynolds number observed in runs A–D.

As anticipated before, the lower bound is expected to become more and more relevant as we approach large Reynolds numbers. However, validating this expectation by a direct numerical simulation, including the proper number of droplets and the whole range of space–time scales involved, is not possible. Instead, we present a direct numerical simulation, labeled run E, designed to reproduce the large-scale parameters typical of a cloud core of size $L = 100$ m: the large-scale eddy turnover time is $T_L \approx 150\ s$, the velocity root-mean-square value is $v_{rms} \approx 0.6$ m s^{-1}, and the mean kinetic energy dissipation is $\varepsilon = 10^{-3}$ m^2 s^{-3}. For this larger cloud core, the supersaturation standard deviation at initial time is $\sigma_s^0 \approx 2\%$: this is consistent with the scaling behavior $\sigma_s^0 \propto A_1 L$ shown in Fig. 1 for runs A–D. The goal of this further experiment is to verify that at larger volumes and longer time scales (T_L is now much larger than τ_s), the quasi-steady approximation for the vapor fluctuations holds and the spectral broadening approaches the lower bound (9). Of course, the small-scale parameters do not match the realistic ones: in this run the smallest resolved scales are $\eta \approx 25$ cm and $\tau_\eta \approx 4$ s, and the turbulence Reynolds number is $Re_\lambda = 185$. Droplets have initial radius 13 μm, as in series 1, and the numerical resolution is $N^3 = 256^3$ grid points. We remark that starting from droplets with initial radius $R = 5$ μm, as in series 2, implies that several droplets evaporate during the simulation. We do not present these results because the complete evaporation of droplets would require a detailed evaluation of the nucleation phase that we neglect here.

Space–time integration of the system has the same features described in section 3, and reference values for the physical parameters entering the model equations are those listed in Table 1.

Clearly, we cannot follow the evolution of 130 cm^{-3} droplets: they would sum up to $N^* = 1.3 \times 10^{14}$. The traditional cloud physics approach avoids this problem by focusing on a number density function representing the local concentration of droplets with a given size (see, e.g., Andrejczuk et al. 2004; Jeffery et al. 2007). However, a complete continuous description for the turbulent transport of inertial particles is still an open issue (see Boffetta et al. 2007 and references therein). Although more computationally demanding, a Lagrangian approach turns out to be more appropriate. We choose then to consider the complete evolution of a subset N_{drops} of droplets, representative of the whole population. Of course, the whole population would absorb, for condensation, more vapor than the representative subset does; therefore, an algorithm is needed to account for the correct feedback of droplets on the supersaturation field. To accomplish this task, we simply normalize the field τ_s with a factor N^*/N_{drops}. Details on the meaning and the convergence of this simple algorithm are discussed in appendix A.

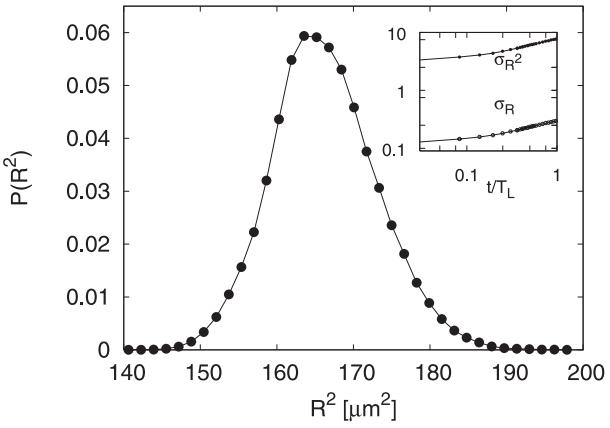

FIG. 4. Droplet square size distribution $P(R^2)$ measured after one large-scale eddy turnover time $T_L \sim 150$ s for run E, matching the large-scale cloud parameters. Inset: time evolution of the standard deviation of the radius distribution $\sigma_R(t)$ and the square radius distribution $\sigma_{R^2}(t)$. At time $t = T_L$, we measure $\sigma_R(T_L) \simeq 0.30 \pm 0.04$ μm and $\sigma_{R^2}(T_L) \simeq 7.5 \pm 1\ \mu m^2$.

At droplet injection, the supersaturation fluctuations for simulation E start with $\sigma_s^0 \sim A_1 w_{rms} T_L \approx 2\%$; after a few vapor phase relaxation times they are depleted to $\sigma_s^{qs} \sim A_1 w_{rms} \tau_s \approx 0.04\%$ and oscillate around this value at later times. Droplets thus experience for most of the evolution a supersaturation level close to the quasi-steady value, which validates the lower bound scenario. The relevant spreading of the square size distribution shown in Fig. 4 can be quantified in terms of the standard deviation of the radius and of the square radius. After one large-scale eddy turnover time, we obtain $\sigma_R(T_L) \simeq 0.30 \pm 0.04$ μm and $\sigma_{R^2}(T_L) \simeq 7 \pm 1\ \mu m^2$, respectively. Although simulation E cannot resolve the whole range of spatial scales of turbulence, by matching the parameters on the large scales of the problem it is able to reproduce the intensity of the large-scale fluctuations.

The final spreading achieved is very close to the lower bound, obtained above by assuming that the supersaturation fluctuations stabilize to σ_s^{qs} and rapidly forget their initial condition. This is consistent with the picture

drawn and supports the observation that the lower bound is more relevant when dealing with large space–time scales. The result suggests that this could be the case for large Reynolds number turbulence. Let us remark, however, that care must be taken in this respect because the spatiotemporal complexity of turbulence at $\mathrm{Re}_\lambda \approx 5000$ is not described by the direct numerical simulation E here presented.

A direct comparison with in situ measurements is not possible because the properties of cloud turbulence and fluctuate considerably. Several broadening mechanisms are likely to occur simultaneously and it is hard to distinguish between them through in situ measurements [see discussion in Brenguier and Chaumat (2001)]. Moreover, we are targeting a cloud core of 100 m because of consistency of the approximations made in the model, but this choice of the size is conservative and somewhat arbitrary. Realistic values are typically one order of magnitude larger where we cannot venture our dimensional analysis. For the sake of completeness we recall, however, that in Brenguier and Chaumat (2001) the authors analyze samples of narrow spectra selected in nonprecipitating cumulus clouds. Measurements of droplet spectral broadening, together with the discussion of the instrumental artifacts, can be found for samples at altitudes of about 1500 m over the cloud base and with droplet concentrations between 200 and 450 cm^{-3}.

6. Conclusions and perspectives

Turbulent fluctuations have been shown to play a crucial role in the broadening of the droplet-size distribution in an idealized setting for condensation in warm adiabatic cloud cores. A qualitative explanation for this observation relies on the nontrivial spatial structure typical of turbulent fields. Large eddies can trap droplets in strong vertical displacements, producing relevant supersaturation fluctuations. The different growth histories resulting from these extreme events yield the observed size-spectrum broadening. The effect is expected to grow with the size of the cloud, since this allows droplets to get trapped in longer updrafts. We confirm this expectation by means of two series of direct numerical simulations up to $\mathrm{Re}_\lambda \sim 185$ and with millions of droplets. In particular, we quantify the increase of broadening as a function of the microscale Reynolds number, a measure of the range of spatial scales of turbulence.

The general outcome of this result is that the role of turbulence for condensation in clouds may not be assessed just by focusing on small Reynolds numbers, where a limited range of spatial scales is considered. This is the case for fluid parcel models, which in fact do not represent a portion of a large cloud but rather a very small cloud. In a real cloud, droplets are brought close to one another by turbulence, but they previously experience disparate supersaturation fluctuations, much stronger than the tiny ones occurring in a single parcel. The results that we obtain at moderate Reynolds number are consistent with those found in Vaillancourt et al. However, as already pointed out, the spectral broadening may achieve relevant values at high Reynolds numbers.

Therefore, a strategy must be conceived to extrapolate the results of DNS or laboratory experiments that cannot achieve the extreme Reynolds numbers of real cloud turbulence. To get a better intuition on this point, we perform a dimensional analysis of the final broadening viewed as a function of the Reynolds number. At moderate Re_λ it is possible to neglect the feedback of droplets on the vapor field. This yields a dimensional expectation consistent with the DNS data.

At larger Reynolds numbers, however, droplets are expected to consistently modify the surrounding vapor field. Therefore, the extrapolation of the abovementioned dimensional behavior provides an upper bound to the actual spectral broadening at large Reynolds numbers. At extremely high Reynolds numbers the upper bound is expected to largely overestimate the actual spectral broadening. Based on the quasi-steady approximation for the vapor field, we propose a correction to estimate the effective absorption of vapor for condensation at large Reynolds numbers, yielding a lower bound on the spectral broadening. The quasi-steady estimate is expected to hold for time scales much larger than the time scale of vapor absorption. A further simulation designed to discuss the validity of this argument shows that at large space–time scales the final broadening is well approximated by the lower bound. This suggests, within the limits of simple dimensional arguments, that the lower bound could be a good candidate to estimate the size-spectra broadening at large Reynolds numbers.

In this work, we focused on the role of turbulence for droplet condensation at moderate to high Reynolds numbers. To enlighten the basic mechanisms yielded by turbulence, we considered a simple model describing the essential physical processes. The underlying assumptions are expected to hold up to spatial scales on the order of hundreds of meters. This prevents us from directly comparing the results with in situ measurements because cloud cores are typically kilometers in size. More sophisticated models have been proposed in the literature accounting for additional microphysical and thermodynamic couplings. Ingredients such as the explicit dependence of the vapor field on the

temperature fluctuations, the microscopic interactions of droplets with the turbulent fields, and the role of buoyancy both at small and large scales may yield corrections to the presented results. Other aspects (such as the small-scale intermittent nature of the velocity and vapor fields, droplet preferential concentration, and modified relative velocity effects) were not specifically addressed in this work, although they are in fact included in the model. Preferential concentration and relative velocity effects, in particular, have been associated with the efficiency of collision/coalescence processes (see Wang et al. 2005; Falkovich et al. 2002; Wilkinson et al. 2006) before they become dominated by gravity.

The problem considered here clearly deserves further theoretical, experimental, and numerical insight and represents a promising challenge for future research. In particular, the ideas at the basis of this work could be verified and complemented through laboratory experiments.

Acknowledgments. We acknowledge discussions with Antonio Celani and Andrea Mazzino, who have inspired and motivated this work. We also acknowledge useful comments received from Prof. Wojciech Grabowski. AS was partially supported by a L'Oréal Italia—Unesco for Women in Science Fellowship and by the HPC–Europa Transnational Access Program. AL acknowledges discussions with Dr. Andrea Buzzi and support from CNR Grant ''Short-Term Mobility''. Numerical simulations were performed at the supercomputing center CINECA (Italy). Raw data from our numerical simulations can be downloaded freely from the Web site of the iCFDdatabase (http://cfd.cineca.it).

APPENDIX

Renormalization of Droplet Populations

Simulation E is designed to describe a volume of $(100\ \mathrm{m})^3$ with 130 cm^{-3} droplets. A major drawback of this simulation is that it cannot describe turbulence structure at the smallest scales, below $\eta = 25$ cm and $\tau_\eta = 4$ s. Also, it cannot follow the individual history of the correct number of droplets. This might influence the statistics of vapor fluctuations because the correct feedback of droplets on the vapor field is not accounted for. In particular, a concentration of 130 cm^{-3} droplets yields a total number of particles $N^* \approx 10^{14}$, whereas we consider the evolution of several million droplets (N_{drops}) because of computational limits. Clearly, 10^{14} droplets would absorb much more vapor for condensation than a few millions do; thus, an algorithm is needed to account for this. The simplest way to estimate the feedback of the whole population on the supersaturation field is to normalize τ_s with a factor N_{drops}/N^*. This amounts to considering each droplet as representing N^*/N_{drops} *equal* particles in the same volume $(\delta x)^3$, where $\delta x \approx 25$ cm.

To evaluate the reliability of this approach, we must consider the single grid cell. If there is one representative drop per cell, the algorithm computes the feedback on vapor as if the average size of droplets in the cell were exactly the radius of that unique representative. On the contrary, a volume of $(25\ \mathrm{cm})^3$—the grid cell size in simulation E—should contain several droplets spanning a whole size spectrum whose mean value is not well represented by one single droplet. Of course, a higher number of particles would better represent the local mean radius, and we expect the algorithm to

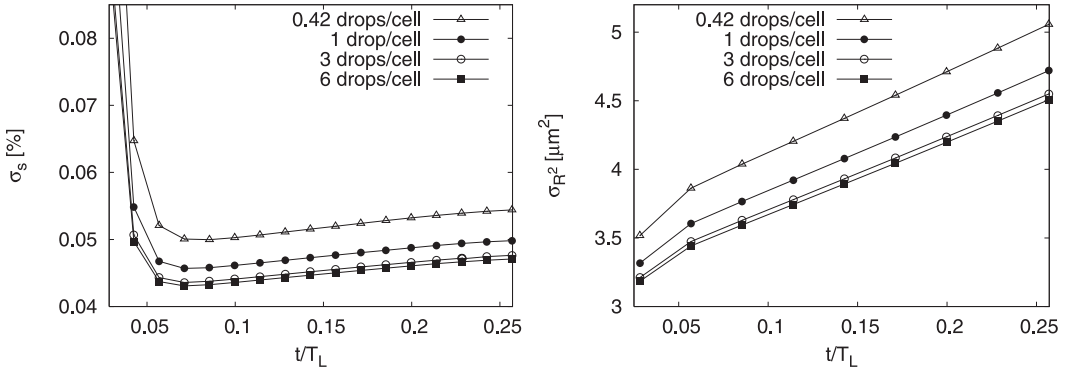

FIG. A1. (left) Supersaturation standard deviation as a function of time. (right) Standard deviation of droplet radius squared σ_{R^2} as a function of time. Results are shown for simulation E, with four different numbers of droplets N_{drops} representative of a population of $N^* \approx 10^{14}$ droplets. The feedback of the whole population on the supersaturation field is accounted for by renormalizing τ_s with a factor N^*/N_{drops} (see text). The algorithm converges when the number of representative droplets is larger than one per cell.

converge for density values larger than one droplet per cell. We test this expectation by repeating simulation E for a time lag $t = T_L/4$, with 0.4, 1, 3, and 6 droplets per grid cell, corresponding to a total number of $N_{\text{drops}} \approx 7$, 17, 50, and 100 million droplets, respectively. Consistently, we use different renormalization factors N^*/N_{drops}. On average, the supersaturation phase relaxation time scale τ_s is the same in the four simulations (not shown), pointing to a correct renormalization.

In the left panel of Fig. A1, the four standard deviations of the supersaturation field are shown in time. They all start with the same initial value (about $A_1 w_{\text{rms}} T_L \approx 2\%$; not shown) and relax to a value of the order of $A_1 w_{\text{rms}} \tau_s$, with some differences for the different concentrations of representative droplets. These deviations decrease when the number of representative droplets increases, showing that the algorithm renormalizing the feedback of droplets on vapor converges. Consistently, the evolution of the spectral broadening (shown in the right panel of Fig. 5) tends to collapse to a unique curve when the number of droplets per cell is larger than one. According to this analysis, we choose to perform the complete simulation, lasting one large-scale eddy turnover time, with one and three droplets per cell, corresponding to a total number of about 17 and 50 million droplets, respectively. The error bar on the final broadening is estimated from these two runs.

REFERENCES

Andrejczuk, M., W. W. Grabowski, S. P. Malinowski, and P. K. Smolarkiewicz, 2004: Numerical simulations of cloud–clear air interfacial mixing. *J. Atmos. Sci.,* **61,** 1726–1739.

Bartlett, J. T., and P. R. Jonas, 1972: On the dispersion of the sizes of droplets growing by condensation in turbulent clouds. *Quart. J. Roy. Meteor. Soc.,* **98,** 150–164.

Blyth, A., 1993: Entrainment in cumulus clouds. *J. Appl. Meteor.,* **32,** 626–641.

Boffetta, G., A. Celani, F. D. Lillo, and S. Musacchio, 2007: The Eulerian description of dilute collisionless suspension. *Europhys. Lett.,* **78,** 14001, doi:10.1209/0295-5075/78/14001.

Brenguier, J.-L., and L. Chaumat, 2001: Droplet spectra broadening in cumulus clouds. Part I: Broadening in adiabatic cores. *J. Atmos. Sci.,* **58,** 628–641.

Celani, A., G. Falkovich, A. Mazzino, and A. Seminara, 2005: Droplet condensation in turbulent flows. *Europhys. Lett.,* **70,** 775–781.

——, A. Mazzino, A. Seminara, and M. Tizzi, 2007: Droplet condensation in convective turbulence. *J. Turbul.,* **8,** 1–9.

Chaumat, L., and J.-L. Brenguier, 2001: Droplet spectra broadening in cumulus clouds. Part II: Microscale droplet concentration heterogeneities. *J. Atmos. Sci.,* **58,** 642–654.

Chen, S., G. D. Doolen, R. H. Kraichnan, and Z.-S. She, 1993: On statistical correlations between velocity increments and locally averaged dissipation in homogeneous turbulence. *Phys. Fluids,* **5A,** 458–463.

Clark, T. L., and W. D. Hall, 1979: A numerical experiment on stochastic condensation theory. *J. Atmos. Sci.,* **36,** 470–483.

Cooper, W. A., 1989: Effects of variable droplet growth histories on droplet size distributions. Part I: Theory. *J. Atmos. Sci.,* **46,** 1301–1311.

Eaton, J. K., and J. R. Fessler, 1994: Preferential concentrations of particles by turbulence. *Int. J. Multiphase Flow,* **20,** 169–209.

Falkovich, G., A. Fouxon, and M. G. Stepanov, 2002: Acceleration of rain initiation by cloud turbulence. *Nature,* **419,** 151–154.

Frisch, U., and A. Nikolaevich, 1995: *Turbulence*. Cambridge University Press, 296 pp.

Grabowski, W. W., and P. Vaillancourt, 1999: Comments on ''Preferential concentration of cloud droplets by turbulence: Effects on the early evolution of cumulus cloud droplet spectra.'' *J. Atmos. Sci.,* **56,** 1433–1436.

Houghton, J. T., and Coauthors, Eds., 2001: *Climate Change 2001: The Scientific Basis*. Cambridge University Press, 881 pp.

Jeffery, C. A., J. M. Reisner, and M. Andrejczuk, 2007: Another look at stochastic condensation for subgrid clous modeling: Adiabatic evolution and effects. *J. Atmos. Sci.,* **64,** 3949–3968.

Korczyk, P., P. Malinowski, and T. A. Kowalewski, 2006: Mixing of cloud and clear air in centimeter scales observed in laboratory by means of particle image velocimetry. *Atmos. Res.,* **82,** 173–182.

Korolev, A. V., and I. P. Mazin, 2003: Supersaturation of water vapor in clouds. *J. Atmos. Sci.,* **60,** 2957–2974.

Lasher-Trapp, S. G., W. Cooper, and A. M. Blyth, 2005: Broadening of droplet size distributions from entrainment and mixing in a cumulus cloud. *Quart. J. Roy. Meteor. Soc.,* **131,** 195–220.

Levin, L. M., and Y. S. Sedunov, 1966: Stochastic condensation of drops and kinetics of cloud spectrum formation. *J. Rech. Atmos.,* **2,** 425–432.

Malinowski, S. P., I. Zawadzki, and P. Banat, 1998: Laboratory observations of cloud–clear air mixing in small scales. *J. Atmos. Oceanic Technol.,* **15,** 1060–1065.

Martonen, T. B., 2000: *Medical Applications of Computer Modelling: Cardiovascular and Ocular Systems*. WIT Press, 290 pp.

Maxey, M. R., and J. Riley, 1983: Equation of motion for a small rigid sphere in a nonuniform flow. *Phys. Fluids,* **26,** 883–889.

Mazin, I. P., 1968: The stochastic condensation and its effect on the formation of cloud droplet size distribution. *Proc. Int. Conf. on Cloud Physics,* Toronto, ON, Canada, Amer. Meteor. Soc., 67–71.

Orszag, S., 1971: On the elimination of aliasing in finite-difference schemes by filtering high-wavenumber components. *J. Atmos. Sci.,* **28,** 1074.

Politovich, M. K., and W. A. Cooper, 1988: Variability of the supersaturation in cumulus clouds. *J. Atmos. Sci.,* **45,** 1651–1664.

Pope, S. B., 2000: *Turbulent Flows*. Cambridge University Press, 771 pp.

Pruppacher, H. R., and J. D. Klett, 1997: *Microphysics of Clouds and Precipitation*. Kluwer Academic, 954 pp.

Shaw, R. A., 2003: Particle–turbulence interactions in atmospheric clouds. *Annu. Rev. Fluid Mech.,* **35,** 183–227.

Shraiman, B. I., and E. D. Siggia, 2000: Scalar turbulence. *Nature,* **405,** 639–646.

Spyksma, K., P. Bertello, and M. K. Yau, 2006: A Boussinesq moist turbulence model. *J. Turbul.,* **7,** 1–24.

Srivastava, R. C., 1989: Growth of cloud drops by condensation: A criticism of currently accepted theory and a new approach. *J. Atmos. Sci.,* **46,** 869–887.

Stevens, B., 2005: Atmospheric moist convection. *Annu. Rev. Earth Planet. Sci.,* **33,** 605–643.

Tennekes, H., and J. L. Lumley, 1972: *A First Course in Turbulence*. MIT Press, 300 pp.

Twomey, S., 1959: The nuclei of natural cloud formation. Part II: The supersaturation in natural clouds and the variation of cloud droplet concentration. *Pure Appl. Geophys.,* **43,** 243–249.

Vaillancourt, P. A., and M. K. Yau, 2000: Review of particle–turbulence interactions and consequences for cloud physics. *Bull. Amer. Meteor. Soc.,* **81,** 285–298.

——, ——, and W. W. Grabowski, 2001: Microscopic approach to cloud droplet growth by condensation. Part I: Model description and results without turbulence. *J. Atmos. Sci.,* **58,** 1945–1964.

——, ——, P. Bartello, and W. W. Grabowski, 2002: Microscopic approach to cloud droplet growth by condensation. Part II: Turbulence, clustering, and condensational growth. *J. Atmos. Sci.,* **59,** 3421–3435.

Wang, L.-P., O. Ayala, S. Kasprzak, and W. W. Grabowski, 2005: Theoretical formulation of collision rate and collision efficiency of hydrodynamically interacting cloud droplets in turbulent atmosphere. *J. Atmos. Sci.,* **62,** 2433–2450.

Warner, J., 1969: The microstructure of cumulus clouds. Part I: General features of the droplet spectrum. *J. Atmos. Sci.,* **26,** 1049–1059.

Wilkinson, M., B. Mehlig, and V. Bezuglyy, 2006: Caustic activation of rain showers. *Phys. Rev. Lett.,* **97,** 048501, doi:10.1103/PhysRevLett.97.048501.

Yeung, P. K., and S. B. Pope, 1988: An algorithm for tracking fluid particles in numerical simulations of homogeneous turbulence. *J. Comput. Phys.,* **79,** 373–416.

Zhao, F., M.-C. Lai, and D. L. Harrington, 1999: Automotive spark-ignited direct-injection gasoline engines. *Prog. Energy Combust. Sci.,* **25,** 437–562.